Accepted Manuscript

Sample-based and sample-aggregated based Galerkin projection schemes for structural dynamics

S.E. Pryse, S. Adhikari, A. Kundu

PII: S0266-8920(17)30123-6
DOI: https://doi.org/10.1016/j.probengmech.2017.09.002
Reference: PREM 2942

To appear in: *Probabilistic Engineering Mechanics*

Received date : 12 June 2017
Revised date : 8 September 2017
Accepted date : 20 September 2017

Please cite this article as: S.E. Pryse, S. Adhikari, A. Kundu, Sample-based and sample-aggregated based Galerkin projection schemes for structural dynamics, *Probabilistic Engineering Mechanics* (2017), https://doi.org/10.1016/j.probengmech.2017.09.002

Available online at www.sciencedirect.com

ScienceDirect

Probabilistic Engineering Mechanics 00 (2017) 1–30

Probabilistic Engineering Mechanics

Sample-based and sample-aggregated based Galerkin projection schemes for structural dynamics

S E Pryse[a,*], S Adhikari[a], A Kundu[b]

[a] *Zienkiewicz Centre for Computational Engineering, College of Engineering, Swansea University, Swansea SA1 8EN, UK*

[b] *Applied and Computational Mechanics, Cardiff School of Engineering, Queen's building, The Parade, Cardiff CF24 3AA, UK*

Abstract

A comparative study of two new Galerkin projection schemes to compute the response of discretized stochastic partial differential equations is presented for discretized structures subjected to static and dynamic loads. By applying an eigen-decomposition of a discretized system, the response of a discretized system can be expressed with a reduced basis of eigen-components. Computational reduction is subsequently achieved by approximating the random eigensolutions, and by only including dominant terms. Two novel error minimisation techniques have been proposed in order to lower the error introduced by the approximations and the truncations: a) Sample-based Galerkin projection scheme, b) Sample-aggregated based Galerkin projection scheme. These have been applied through introducing unknown multiplicative scalars into the expressions of the response. The proposed methods are applied to analyse the bending of a cantilever beam with stochastic parameters undergoing both a static and a dynamic load. For the static case the response is real, however the response for the case of a dynamic loading is complex and frequency-dependent. The results obtained through the proposed approaches are compared with those obtained by utilising a direct Monte Carlo approach.

Keywords: Stochastic differential equations; eigenfunctions; Galerkin; projection; reduced methods.

1. Introduction

The mathematical models and the parameters used to model physical systems are idealizations of physical processes. They cannot often be known for certain, and a degree of randomness is involved. In fact, input uncertainty in the form of material parameters, geometrical configuration or boundary conditions are ubiquitous and intrinsic to the models being analysed. Many civil engineering problems are concerned with materials that are

*Corresponding author. Tel: +44 (0)1792 602088, Fax: + 44 (0)1792 295676
Email address: 656060@swansea.ac.uk (S E Pryse)

intrinsically random and merely using the average value or the best possible deterministic values of the material properties would not establish their behaviour with desired confidence or reliability. Fortunately, the entire subject of uncertainty can itself be addressed in a scientific and a mathematically precise way by utilising stochastic computational models.

This work proposes and compares new reduced order methods to approximate the response of stochastic discretized equations. Stochastic sampling techniques which employ Monte Carlo type simulations have been widely used to solve such systems [1, 2]. However the convergence of such methods can be deemed slow. In order to lower the computational cost numerous methods have been suggested. These include principal component analysis [3], quasi Monte Carlo [4] and Latin hypercube sampling [5]. A comprehensive review of sampling techniques is given by [6]. In spite of the slow convergence rate, brute force Monte Carlo simulations are often treated as a benchmark solution in stochastic computational mechanics literature e.g. [7].

Expansion methods have also been utilised for computing the response of stochastic structures. Such methods include the perturbation method [8, 9] and Neumann series [10, 11]. A perturbation method expands a systems solution by using a Taylor series whilst the Neumann series method approximates the inverse of the stochastic matrices with a Neumann type matrix series expansion. Projection methods have also been used for solving stochastic equations. Originating from [12], [13] have proposed a polynomial chaos expansion (PCE) for stochastic finite elements which produces a linear combination of Hermite polynomials and undetermined deterministic coefficients. Numerous studies have applied the PCE including [14] and [15]. In turn a generalised PCE approach has been proposed [16, 17] based upon the Wiener-Askey chaos expansion. [18, 19] have explored projections onto preconditioned stochastic Krylov basis functions whilst [20] has utilised a random eigenfunction expansion method to formulate a random basis. Further methods such as stochastic collocation techniques [21, 22] and meta-modelling schemes [23, 24] and reduced stochastic spectral function approach [25, 26] have been suggested when a stochastic finite element analysis of a structural dynamic system is performed. A comprehensive review of the available literature is not given in this paper, however

we refer the reader to [27, 28] for a wide-ranging review of the available reduced order methods.

If the PCE were used, both the static and dynamic cases would use the same projections. In turn this introduces additional problems into the computation [29]. This paper aims to discuss projection methods which are specificity designed to capture the physical nature of the systems. By applying a random eigenfunction approach a comparative study between two novel Galerkin projection schemes (a) A sample-based Galerkin projection scheme and (b) A sample-aggregated based Galerkin projection scheme are presented. After applying appropriate computational reduction methods, the two novel Galerkin projection schemes are introduced to a system undergoing a static load and to a system subjected to a dynamic load. The system subjected to a dynamic load is analysed in the frequency domain. The methods are consequently applied to a cantilever beam and their effectiveness are compared. These comparisons are based upon relative error estimates with respect to a benchmark direct Monte Carlo approach.

A brief outline of the formulation of stochastic structural systems is given in Section 2. The relevant projection methods for both loading cases are derived in Section 3 before two methods for reducing the computational cost are discussed in Section 4. As a result of the induced error due to the computational reduction, Section 5 introduces the novel Galerkin projection schemes. The methods are subsequently applied to analyse the bending of a Euler-Bernoulli cantilever beam in Section 6 before the major conclusions are drawn in the concluding section.

2. Formulating the discretized systems

In this work, stochastic discretized equations are considered for structures which are subjected to both static and dynamic loads. This section aims to give a brief overview of the stochastic discretized equations considered to describe structures which are subjected to both static and dynamic loads. The stochastic discretized equations can be obtained by utilising a stochastic finite element approach on a partial differential equation. The technical details of obtaining the discretized set of equations have been omitted, however many references are available on this topic [13].

2.1. Discretized system: Static load

The case of a structure undergoing a static load can be described by the following set of stochastic discretized equations

$$\mathbf{K}(\theta)\mathbf{u}_S(\theta) = \mathbf{f}_0 \tag{1}$$

where $\mathbf{K}(\theta), \mathbf{u}_S(\theta)$ and $\mathbf{f}_0$ correspond to a random stiffness matrix, the response vector and a deterministic excitation field respectively. The discretized set of stochastic linear equations given by Equation (1) can be expressed as follows

$$\mathbf{K}(\theta)\mathbf{u}_S(\theta) = \left[\mathbf{K}_0 + \sum_{j=1}^{M_1} \xi_j(\theta)\mathbf{K}_j\right]\mathbf{u}_S(\theta) = \mathbf{f}_0 \tag{2}$$

$\mathbf{K}_0 \in \mathbb{R}^{N\times N}$ is a positive definite, symmetric matrix which contributes to the deterministic nature of the random stiffness matrix. In a similar manner $\mathbf{K}_j \in \mathbb{R}^{N\times N}$ are general matrices for $j = 1, 2, ...M_1$ which contribute to the stochastic nature of $\mathbf{K}(\theta)$. The function $\xi_j(\theta)$ corresponds to a set of random variables for $j = 1, 2, ...M_1$. The methods proposed in this paper are general in nature, therefore the random variables are not restricted to a specific distribution. A benchmark solution to the set of stochastic linear equations given above can be obtained through direct Monte Carlo simulations [DMCS]

$$\mathbf{u}_S(\theta) = \left[\mathbf{K}_0 + \sum_{j=1}^{M_1} \xi_j(\theta)\mathbf{K}_j\right]^{-1}\mathbf{f}_0 \tag{3}$$

Convergence is guaranteed if all realisations of $\mathbf{K}(\theta)$ are positive definite and the number of realizations is sufficiently large. Equation (3) would subsequently be solved for each $\theta \in \Theta$.

2.2. Discretized system: Dynamic load

The following set of stochastic discretized equations can be used to represent a viscously damped structure undergoing a dynamic load in the frequency domain [30]

$$[-\omega^2\mathbf{M}(\theta) + \mathrm{i}\omega\mathbf{C}_0 + \mathbf{K}(\theta)]\mathbf{u}_D(\omega, \theta) = \tilde{\mathbf{f}}_0(\omega) \tag{4}$$

where $\mathbf{M}(\theta), \mathbf{K}(\theta)$ and $\mathbf{C}_0$ are matrices that correspond to a systems' random mass and stiffness matrices and a systems' deterministic damping matrix respectively. The vector $\tilde{\mathbf{f}}_0$

is a deterministic excitation field, ω is a frequency in the frequency space Ω and $\mathrm{i} = \sqrt{-1}$. The vector $\mathbf{u}_D$ corresponds to the complex dynamic response vector. For both the static and dynamic loading cases $\theta \in \Theta$ is a sample point from the sampling space Θ.

The random variables associated with both the random mass matrix and the random stiffness matrix seen in Equation (4) can be grouped so that $\xi_j(\theta) = \eta_j(\theta)$ for $j = 1, 2, \ldots q_1$ and $\xi_{j+q_1}(\theta) = \nu_j(\theta)$ for $j = 1, 2, \ldots q_2$. Thus the random mass matrix $\mathbf{M}(\theta)$ and random stiffness $\mathbf{K}(\theta)$ can be modelled as:

$$\mathbf{M}(\theta) = \mathbf{M}_0 + \sum_{j=1}^{q_1} \eta_j(\theta)\mathbf{M}_i \in \mathbb{R}^{N\times N} \tag{5}$$

$$\mathbf{K}(\theta) = \mathbf{K}_0 + \sum_{j=1}^{q_2} \nu_j(\theta)\mathbf{K}_i \in \mathbb{R}^{N\times N} \tag{6}$$

$\mathbf{M}_0 \in \mathbb{R}^{N\times N}$ and $\mathbf{K}_0 \in \mathbb{R}^{N\times N}$ are the deterministic contributions to the mass and stiffness matrices, whilst $\mathbf{M}_j \in \mathbb{R}^{N\times N}$ and $\mathbf{K}_j \in \mathbb{R}^{N\times N}$ are the corresponding stochastic contributions. Similarly to the static case, we assume a deterministic excitation vector $\tilde{\mathbf{f}}_0 \in \mathbb{R}^N$. The matrix $\mathbf{C}_0 \in \mathbb{R}^{N\times N}$ is a deterministic damping matrix. For this study, we consider constant modal damping [30], therefore the damping matrix $\mathbf{C}_0$ takes the following form

$$\mathbf{C}_0 = 2\boldsymbol{\zeta}\mathbf{M}_0\sqrt{\mathbf{M}_0^{-1}\mathbf{K}_0} \tag{7}$$

where $\boldsymbol{\zeta}$ denotes a diagonal matrix which contains the modal damping factors

$$\boldsymbol{\zeta} = \mathrm{diag}[\zeta_1, \zeta_2, \ldots \zeta_N] \in \mathbb{R}^{N\times N} \tag{8}$$

As it is assumed that all the diagonal entries are equal it can be deduced that $\zeta_1 = \zeta_2 = \cdots = \zeta_N$. After combining the above expressions, Equation (4) can be expressed as

$$\left[\mathbf{D}_0(\omega) + \sum_{j=1}^{M_2} \xi_j(\theta)\mathbf{D}_j(\omega)\right]\mathbf{u}_D(\omega,\theta) = \tilde{\mathbf{f}}_0(\omega) \tag{9}$$

where $\mathbf{D}_0 \in \mathbb{C}^{N\times N}$ represents the complex deterministic part of the system and $\mathbf{D}_j \in \mathbb{R}^{N\times N}$ the random components. The total number of random variables, M_2, can be computed through summing q_1 and q_2. For the given configuration, the expressions for $\mathbf{D}_0$ and $\mathbf{D}_j$ are as follows

$$\mathbf{D}_0(\omega) = -\omega^2\mathbf{M}_0 + \mathrm{i}\omega\mathbf{C}_0 + \mathbf{K}_0 \tag{10}$$

$$\begin{aligned}\mathbf{D}_j(\omega) &= -\omega^2\mathbf{M}_j \qquad \text{for} \quad j = 1, 2, \ldots, q_1 \\ \mathbf{D}_j(\omega) &= \mathbf{K}_{j-q_1} \qquad \text{for} \quad j = q_1+1, q_1+2, \ldots, q_1+q_2\end{aligned} \tag{11}$$

In the subsequent sections, a reduced order projection method is presented in conjunction with two different Galerkin methods. In order to compare the accuracy of the different methods, a benchmark solution is produced by directly solving Equation (4) [DMCS]

$$\mathbf{u}_D(\omega,\theta) = \left[\mathbf{D}_0(\omega) + \sum_{j=1}^{M_2} \xi_j(\theta)\mathbf{D}_j(\omega)\right]^{-1} \tilde{\mathbf{f}}_0(\omega) \tag{12}$$

This above expression is solved for each $\theta \in \boldsymbol{\Theta}$ and for every frequency value $\omega \in \Omega$.

3. Stochastic projection methods

In this section two stochastic projection methods are discussed to calculate the responses of Equations (2) and (9). We aim to represent these responses by projecting random scalars onto random bases. In turn, the following stochastic projections will form a foundation for the proposed Galerkin approaches

$$\mathbf{u}_S(\theta) = \sum_{j=1}^{N} \alpha_j(\theta)\mathbf{a}_j(\theta) \quad \text{and} \quad \mathbf{u}_D(\omega,\theta) = \sum_{j=1}^{N} \beta_j(\omega,\theta)\mathbf{b}_j(\theta) \tag{13}$$

For the case of a static load, $\alpha_j(\theta) \in \mathbb{R}^N$ denotes the random scalars and $\mathbf{a}_j(\theta) \in \mathbb{R}^{N\times N}$ the random basis. Likewise for the case of a dynamic load, $\beta_j(\omega,\theta) \in \mathbb{C}^N$ denotes the random scalars and $\mathbf{b}_j(\theta) \in \mathbb{R}^{N\times N}$ the random basis. The stochastic projection method for the case of a static load is initially considered.

3.1. Stochastic projection: Static load

In order to obtain an expression for the response in the same form as Equation (13) we initially consider the following random eigenvalue problem

$$\mathbf{K}(\theta)\boldsymbol{\phi}_k(\theta) = \lambda_k(\theta)\boldsymbol{\phi}_k(\theta); \quad k = 1, 2, \ldots N \tag{14}$$

For convenience, the matrices of the random eigenvalues and eigenvectors of $\mathbf{K}(\theta)$ are defined as follows

$$\begin{aligned}\boldsymbol{\Lambda}(\theta) &= \text{diag}\left[\lambda_1(\theta), \lambda_2(\theta), \ldots, \lambda_N(\theta)\right] \in \mathbb{R}^{N\times N} \quad \text{and} \\ \boldsymbol{\Phi}(\theta) &= \left[\boldsymbol{\phi}_1(\theta), \boldsymbol{\phi}_2(\theta), \ldots, \boldsymbol{\phi}_N(\theta)\right] \in \mathbb{R}^{N\times N}\end{aligned} \tag{15}$$

The random eigenvalues are arranged in ascending order so $\lambda_1(\theta) < \lambda_2(\theta) < \ldots < \lambda_N(\theta)$. The corresponding eigenvectors are consequently arranged in the same order. Due to the orthogonality of $\mathbf{\Phi}(\theta)$, it is deduced that $\mathbf{\Phi}(\theta)^{-1} = \mathbf{\Phi}(\theta)^T$. Thus the following identities can be defined

$$\mathbf{\Phi}^T(\theta)\mathbf{K}(\theta)\mathbf{\Phi}(\theta) = \mathbf{\Lambda}(\theta); \quad \mathbf{K}(\theta) = \mathbf{\Phi}^{-T}(\theta)\mathbf{\Lambda}(\theta)\mathbf{\Phi}^{-1}(\theta) \quad \text{and} \quad \mathbf{K}^{-1}(\theta) = \mathbf{\Phi}(\theta)\mathbf{\Lambda}^{-1}(\theta)\mathbf{\Phi}^T(\theta) \tag{16}$$

Using these identities, the response of Equation (2) can be expressed as

$$\mathbf{u}_S(\theta) = \left[\mathbf{\Phi}(\theta)\mathbf{\Lambda}^{-1}(\theta)\mathbf{\Phi}^T(\theta)\right]\mathbf{f}_0 = \sum_{j=1}^{N} \frac{\boldsymbol{\phi}_j^T(\theta)\mathbf{f}_0}{\lambda_j(\theta)}\boldsymbol{\phi}_j(\theta) \tag{17}$$

It is apparent that Equation (17) is of the same form as Equation (13). The quantity $\frac{\boldsymbol{\phi}_j^T(\theta)\mathbf{f}_0}{\lambda_j(\theta)}$ corresponds to the scalar term $\alpha_j(\theta)$ and $\boldsymbol{\phi}_j(\theta)$ corresponds to the vector term $\mathbf{a}_j(\theta)$. The number of terms in the summation, N, corresponds to the number of degrees of freedom associated with a structure.

3.2. Stochastic projection: Dynamic load

Similarly to the case of a static load, a random eigenvalue problem is considered in order to represent the response in the form of Equation (13). However contrary to the static case, random stiffness and random mass matrices are taken into consideration

$$\mathbf{K}(\theta)\boldsymbol{\psi}_k(\theta) = \mu_k(\theta)\mathbf{M}(\theta)\boldsymbol{\psi}_k(\theta); \quad k = 1, 2, \ldots N \tag{18}$$

where $\mu_k(\theta)$ and $\boldsymbol{\psi}_k(\theta)$ are the kth undamped random eigenvalue and eigenvector. Matrices that contain the set of undamped random eigenvalues and eigenvectors are defined as follows

$$\begin{aligned} \mathbf{\Omega}^2(\theta) &= \text{diag}\left[\mu_1(\theta), \mu_2(\theta), \ldots, \mu_N(\theta)\right] \in \mathbb{R}^{N\times N} \quad \text{and} \\ \mathbf{\Psi}(\theta) &= \left[\boldsymbol{\psi}_1(\theta), \boldsymbol{\psi}_2(\theta), \ldots, \boldsymbol{\psi}_N(\theta)\right] \in \mathbb{R}^{N\times N} \end{aligned} \tag{19}$$

where the undamped eigenvalues are arranged in ascending order so $\mu_1(\theta) < \mu_2(\theta) < \ldots < \mu_N(\theta)$. The corresponding eigenvectors are subsequently mass normalised and arranged in the same order. It is apparent that the following relationships hold

$$\begin{aligned} \mathbf{\Psi}^T(\theta)\mathbf{M}(\theta)\mathbf{\Psi}(\theta) &= \mathbf{I} \\ \mathbf{\Psi}^T(\theta)\mathbf{K}(\theta)\mathbf{\Psi}(\theta) &= \mathbf{\Omega}^2(\theta) \end{aligned} \tag{20}$$

By combining the above identities with Equation (4) it is possible to gain a representation for the response in the form of Equation (13). We initially define the following modal damping matrix

$$\mathbf{C}'(\theta) = \mathbf{\Psi}^T(\theta)\mathbf{C}_0\mathbf{\Psi}(\theta) = 2\boldsymbol{\zeta}\mathbf{\Omega}(\theta) \tag{21}$$

where $\boldsymbol{\zeta}$ corresponds to the diagonal modal damping matrix introduced in Equation (8). By using the following modal transformation $\mathbf{u}_D(\omega,\theta) = \mathbf{\Psi}(\theta)\bar{\mathbf{y}}(\omega,\theta)$ and by pre-multiplying Equation (4) with $\mathbf{\Psi}^T(\theta)$, we obtain

$$\left[-\omega^2\mathbf{I} + 2\mathrm{i}\omega\boldsymbol{\zeta}\mathbf{\Omega}(\theta) + \mathbf{\Omega}^2(\theta)\right]\bar{\mathbf{y}}(\omega,\theta) = \mathbf{\Psi}^T(\theta)\tilde{\mathbf{f}}_0(\omega) \tag{22}$$

By inverting $\left[-\omega^2\mathbf{I} + 2\mathrm{i}\omega\boldsymbol{\zeta}\mathbf{\Omega}(\theta) + \mathbf{\Omega}^2(\theta)\right]$ and pre-multiplying both sides of the above equation with $\mathbf{\Psi}(\theta)$ it is apparent that

$$\mathbf{\Psi}(\theta)\bar{\mathbf{y}}(\omega,\theta) = \mathbf{\Psi}(\theta)\left[-\omega^2\mathbf{I} + 2\mathrm{i}\omega\boldsymbol{\zeta}\mathbf{\Omega}(\theta) + \mathbf{\Omega}^2(\theta)\right]^{-1}\mathbf{\Psi}^T(\theta)\tilde{\mathbf{f}}_0(\omega) \tag{23}$$

The computational cost of calculating the inverse of $\left[-\omega^2\mathbf{I} + 2\mathrm{i}\omega\boldsymbol{\zeta}\mathbf{\Omega}(\theta) + \mathbf{\Omega}^2(\theta)\right]$ is rather inexpensive due to the diagonal nature of $\left[-\omega^2\mathbf{I} + 2\mathrm{i}\omega\boldsymbol{\zeta}\mathbf{\Omega}(\theta) + \mathbf{\Omega}^2(\theta)\right]$. By reintroducing $\mathbf{u}_D(\omega,\theta)$ for $\mathbf{\Psi}(\theta)\bar{\mathbf{y}}(\omega,\theta)$ a dynamic response in the frequency domain can be obtained

$$\mathbf{u}_D(\omega,\theta) = \mathbf{\Psi}(\theta)\left[-\omega^2\mathbf{I} + 2\mathrm{i}\omega\boldsymbol{\zeta}\mathbf{\Omega}(\theta) + \mathbf{\Omega}^2(\theta)\right]^{-1}\mathbf{\Psi}^T(\theta)\tilde{\mathbf{f}}_0(\omega) \tag{24}$$

This expression can be rewritten in the form of a summation, where N corresponds to the number of degrees of freedom associated with a structure

$$\mathbf{u}_D(\omega,\theta) = \sum_{j=1}^{N}\beta_j(\omega,\theta)\mathbf{b}_j(\theta) = \sum_{j=1}^{N}\left(\frac{\boldsymbol{\psi}_j^T(\theta)\tilde{\mathbf{f}}_0(\omega)}{\mu_j(\theta) - \omega^2 + 2\mathrm{i}\sqrt{\mu_j(\theta)}\omega\zeta}\right)\boldsymbol{\psi}_j(\theta) \tag{25}$$

It is apparent that the response of a system undergoing a dynamic load can be represented in same form as Equation (13). The random scalars, $\beta_j(\omega,\theta)$, correspond to the result of $\frac{\boldsymbol{\phi}_j^T(\theta)\tilde{\mathbf{f}}_0}{\lambda_j(\theta)-\omega^2+2\mathrm{i}\sqrt{\lambda_j(\theta)}\omega\zeta}$. In turn, these random scalars are projected onto the space spanned by $\boldsymbol{\psi}_j(\theta)$.

4. Approaches towards reducing the computational cost

Calculating the exact values of $\alpha_j(\theta)$, $\beta_j(\omega,\theta)$, $\mathbf{a}_j(\theta)$ and $\mathbf{b}_j(\theta)$ could prove difficult, and in turn could be more computationally expensive than solving Equations (3) and (12). This section aims to address this issue by offering two approaches to lower the computational cost:

- The random eigensolutions arising in Equations (17) and (25) can be approximated.
- The number of terms arising in the summations seen in Equations (17) and (25) can be reduced.

By implementing these approaches the computational cost associated with approximating the responses of Equations (2) and (9) will be dramatically lower than the computational cost associated with computing the exact solutions. Approximating the random eigensolutions for the case of a static load is initially considered.

4.1. Approximating the random eigenvalues and eigenvectors

Direct Monte Carlo simulations can be used in collaboration with the random eigenvalue problem in order to calculate the exact values of the random eigenvalues and eigenvectors; however this method is computationally expensive. Numerous methods have been proposed to approximate the random eigensolutions and in turn lower the computational cost. These include a subspace iteration method [31] and a polynomial chaos approach [32]. This work explores the use of a perturbation method to approximate both the random eigenvalues and random eigenvectors.

4.1.1. Approximating the random eigenvalues and eigenvectors: Static load

Solutions of different perturbation methods are obtained by varying the truncation value of a Taylor series expansion. Due to its efficiency and ease, the first order perturbation method has been considered. An approximation of the jth random eigenvalue and its corresponding random eigenvector is given by

$$\lambda_j(\theta) \approx \lambda_{j_0} + \sum_{k=1}^{M_1} \left(\frac{\partial \lambda_j}{\partial \xi_k} \right) \mathrm{d}\xi_k(\theta) \tag{26}$$

$$\text{and} \quad \boldsymbol{\phi}_j(\theta) \approx \boldsymbol{\phi}_{j_0} + \sum_{k=1}^{M_1} \left(\frac{\partial \boldsymbol{\phi}_j}{\partial \xi_k} \right) \mathrm{d}\xi_k(\theta) \tag{27}$$

where $\mathrm{d}\xi_k(\theta)$ is a set of random variables. By differentiating the random eigenvalue equation with respect to ξ_k, pre-multiplying with $\boldsymbol{\phi}_{j_0}^T$ and utilising that $\boldsymbol{\phi}_{j_0}^T \boldsymbol{\phi}_{j_0} = 1$, $\frac{\partial \lambda}{\partial \xi_k}$ can be expressed as

$$\frac{\partial \lambda_j}{\partial \xi_k} = \boldsymbol{\phi}_{j_0}^T \frac{\partial \mathbf{K}}{\partial \xi_k} \boldsymbol{\phi}_{j_0} \tag{28}$$

In the instance of Equation (28), $\frac{\partial \mathbf{K}}{\partial \xi_k} = \mathbf{K}_k$.

The partial derivative of $\boldsymbol{\phi}_j$ with respect to ξ_k can be calculated by expanding $\frac{\partial \phi_j}{\partial \xi_k}$ as a linear combination by utilising deterministic eigenvalues and eigenvectors [33]

$$\frac{\partial \boldsymbol{\phi}_j}{\partial \xi_k} = \sum_{i=1 \neq j}^{N} \alpha_{jki} \boldsymbol{\phi}_i \quad \text{where} \quad \alpha_{jki} = \frac{\boldsymbol{\phi}_{i_0}^T \frac{\partial \mathbf{K}}{\partial \xi_k} \boldsymbol{\phi}_{j_0}}{\lambda_{j_0} - \lambda_{i_0}} \tag{29}$$

In this instance, $\frac{\partial \mathbf{K}}{\partial \xi_k} = \mathbf{K}_k$ and $\alpha_{jki}\boldsymbol{\phi}_i = 0$ when $i = j$. This method requires all the deterministic eigenvalues and eigenvectors to be know and for all the eigenvalues to be distinct. The case of repeated eigenvalues is beyond the scope of this paper.

4.1.2. Approximating the random eigenvalues and eigenvectors: Dynamic load

Similarly to the previous case, the random eigenvalues and eigenvectors for the case of a dynamic load can be approximated by a first order perturbation

$$\mu_j(\theta) \approx \mu_{j_0} + \sum_{k=1}^{M_2} \left(\frac{\partial \mu_j}{\partial \xi_k} \right) \mathrm{d}\xi_k(\theta) \tag{30}$$

$$\text{and} \quad \boldsymbol{\psi}_j(\theta) \approx \boldsymbol{\psi}_{j_0} + \sum_{k=1}^{M_2} \left(\frac{\partial \boldsymbol{\psi}_j}{\partial \xi_k} \right) \mathrm{d}\xi_k(\theta) \tag{31}$$

where μ_{j_0} and ψ_{j_0} are the jth deterministic undamped eigenvalue and eigenvector and $\mathrm{d}\xi_k(\omega)$ a set of random variables. The derivative of the undamped random eigenvalues with respect to ξ_k can be obtained by differentiating and manipulating the random eigenvalue equation denoted by Equation (18) [33]. This results in the following equation

$$\frac{\partial \mu_j}{\partial \xi_k} = \frac{\boldsymbol{\psi}_{0_j}^T \left[\frac{\partial \mathbf{K}}{\partial \xi_k} - \mu_{0_j} \frac{\partial \mathbf{M}}{\partial \xi_k} \right] \boldsymbol{\psi}_{0_j}}{\boldsymbol{\psi}_{0_j}^T \mathbf{M}_0 \boldsymbol{\psi}_{0_j}} \tag{32}$$

where μ_{0_j} and $\boldsymbol{\psi}_{0_j}$ correspond to the deterministic undamped eigenvalues and eigenvectors. Due to the mass normalisation of the undamped eigenvectors, the above denominator equates to one, thus it can be deduced that

$$\frac{\partial \mu_j}{\partial \xi_k} = \boldsymbol{\psi}_{0_j}^T \left[\frac{\partial \mathbf{K}}{\partial \xi_k} - \mu_{0_j} \frac{\partial \mathbf{M}}{\partial \xi_k} \right] \boldsymbol{\psi}_{0_j} \tag{33}$$

The values of both $\frac{\partial \mathbf{M}}{\partial \xi_k}$ and $\frac{\partial \mathbf{K}}{\partial \xi_k}$ seen in Equation (33) are as follows

$$\begin{aligned} \frac{\partial \mathbf{M}}{\partial \xi_k} &= \begin{cases} \mathbf{M}_k, & \text{for } k = 1, 2, \ldots, q_1 \\ 0, & \text{otherwise} \end{cases} \\ \frac{\partial \mathbf{K}}{\partial \xi_k} &= \begin{cases} \mathbf{K}_{k-q_1}, & \text{for } k = q_1+1, q_1+2, \ldots, q_1+q_2 \\ 0, & \text{otherwise} \end{cases} \end{aligned} \tag{34}$$

where $\mathbf{M}_k$ and $\mathbf{K}_{k-q_1}$ correspond to the random components of $\mathbf{M}(\theta)$ and $\mathbf{K}(\theta)$ introduced in Equations (5) and (6). The partial derivative of the random undamped eigenvectors with respect to ξ_k can be expressed by a linear combination of deterministic eigenvectors. The full algebraic detail of obtaining the derivative of the random eigenvectors has been omitted, but can again be found in [33]. The final expression for $\frac{\partial \boldsymbol{\psi}_j}{\partial \xi_k}$ is given by

$$\frac{\partial \boldsymbol{\psi}_j}{\partial \xi_k} = -\frac{1}{2}\left(\boldsymbol{\psi}_{j_0}^T \frac{\partial \mathbf{M}}{\partial \xi_k}\boldsymbol{\psi}_{j_0}\right) + \sum_{i=1\neq j}^{N} \frac{\boldsymbol{\psi}_{k_0}^T\left[\frac{\partial \mathbf{K}}{\partial \xi_k} - \mu_{j_0}\frac{\partial \mathbf{M}}{\partial \xi_k}\right]\boldsymbol{\psi}_{j_0}}{\mu_{j_0} - \mu_{k_0}}\boldsymbol{\psi}_{k_0} \tag{35}$$

where values of both $\frac{\partial \mathbf{M}}{\partial \xi_k}$ and $\frac{\partial \mathbf{K}}{\partial \xi_k}$ are identical to those given in Equation (34). This method also requires all the deterministic eigenvalues and eigenvectors to be known. Furthermore the eigenvalues are required to be unique. The proposed methods would still be valid for the case of repeated eigenvalues, however a different method would be required to approximate the eigenvectors.

4.2. Truncation of the series expansions

At present both the static and dynamic methods described in Section (3) require the calculation and summation of N terms. However a vast number of higher order terms seen in the summations have a relatively low value, therefore further computational reduction can be achieved by removing these low valued terms.

4.2.1. Truncation: Static load

The series given in Equation (17) can be truncated after a certain number of terms. As the eigenvalues have been ordered ascendingly, it can be deduced that the higher order terms arising in the summation have a low value. By retaining the dominant terms, it is hoped that enough terms are retained in order to capture the behaviour of the system.

The number of dominant terms to be retained can either be predefined or determined by a ratio such as:

$$\frac{\lambda_{1_0}}{\lambda_{n_{s0}}} > \varepsilon \tag{36}$$

where λ_{1_0} is the first, and therefore the smallest deterministic eigenvalue and $\lambda_{n_{s0}}$ is the n_s largest deterministic eigenvalue which satisfies the above inequality. The value of n_s would correspond to the number of terms to be kept in the truncation. The value ε is to be selected appropriately. Hence Equation (17) can be truncated as follows

$$\mathbf{u}_S(\omega) \approx \sum_{j=1}^{n_s} \frac{\boldsymbol{\phi}_j^T(\omega)\mathbf{f}_0}{\lambda_j(\omega)}\boldsymbol{\phi}_j(\omega) \tag{37}$$

where $n_s < N$. The full response for $\mathbf{u}_S(\omega)$ can then be obtained by performing a Monte Carlo simulation on each sample.

4.2.2. Truncation: Dynamic load

By combining the ordering of the eigenvalues with the following relationship: $\omega_j(\theta) = \sqrt{\mu_j(\theta)}$ it can be deduced that

$$\omega_1(\theta) < \omega_2(\theta) < \ldots < \omega_N(\theta) \tag{38}$$

where ω_j corresponds to the jth natural frequency. By examining the scalar term $\beta_j(\omega, \theta)$ it can be observed that the natural frequencies appear in the denominator

$$\beta_j(\omega, \theta) = \frac{\boldsymbol{\psi}_j^T(\theta)\tilde{\mathbf{f}}_0}{\omega_j^2(\theta) - \omega^2 + 2\mathrm{i}\omega_j(\theta)\omega\zeta} \tag{39}$$

For the values of j satisfying $\omega_j^2(\theta) + 2\mathrm{i}\omega_j\omega(\theta)\zeta > \omega^2$, it is apparent that the value of the denominator increases as the value of j increases. Therefore it is established that the value of $\beta_j(\omega, \theta)$ generally decreases as the value of j increases. Consequently the upper limits of the summations seen in Equation (25) can be lowered

$$\mathbf{u}_D(\omega, \theta) \approx \sum_{j=1}^{n_d} \left(\frac{\boldsymbol{\psi}_j^T(\theta)\tilde{\mathbf{f}}_0}{\omega_j^2(\theta) - \omega^2 + 2\mathrm{i}\omega_j(\theta)\omega\zeta} \right) \boldsymbol{\psi}_j(\theta) \tag{40}$$

where $n_d < N$. Similarly to a system subject to a static load, the value of n_d can be defined in two ways. The value can be predefined or it can by deduced from the ratio of two eigenvalues (similarly to that seen in Equation (36)). Monte Carlo simulations would subsequently be performed for each $\theta \in \Theta$ and $\omega \in \Omega$.

5. Error minimisation through Galerkin methods

Expressions for computing the response of discretized structures that are subjected to a static or a dynamic load have been proposed. It has been shown that computational reduction can be achieved by approximating eigensolutions and by applying suitable truncations. However these reductions induces error into the calculations. This has motivated an error minimisation approach, and as a consequence, two Galerkin approaches have been considered:

- A sample-aggregated based Galerkin approach [SPAG]
- A sample-based Galerkin approach [SPSG]

By incorporating the Galerkin approaches, this section aims to reduce the error induced due by the approximations and truncations introduced in Section (4). The SPAG approach for the case of a static load is initially considered.

5.1. Sample-aggregated based Galerkin approach: Static load

For this approach, the solution vector is modified to take the following form

$$\mathbf{u}_{SA}(\theta) \approx \sum_{j=1}^{n_s} c_j \left(\frac{\boldsymbol{\phi}_j^T(\theta)\mathbf{f}_0}{\lambda_j(\theta)} \right) \boldsymbol{\phi}_j(\theta) \tag{41}$$

where $\lambda_j \in \mathbb{R}^{n_s}$ and $\boldsymbol{\phi}_j \in \mathbb{R}^{N \times n_s}$ represent the random eigenvalues and eigenvectors, and $\mathbf{f}_0 \in \mathbb{R}^N$ is the deterministic excitation vector. $c_j \in \mathbb{R}^{n_s}$ corresponds to deterministic constants which need to be determined. The residual vector for this the new approach is defined as

$$\mathbf{r}_{SA}(\theta) = \mathbf{K}(\theta)\mathbf{u}(\theta) - \mathbf{f}_0 \tag{42}$$

By making the residual orthogonal to a basis function, the deterministic scalars c_j can be computed. As Equation (23) can be viewed as a projection onto a subset of random eigenvectors, the residual can be made orthogonal to the same subset of random eigenvectors

$$< \mathbf{r}_{SA}(\theta), \boldsymbol{\phi}_k(\theta) > \qquad \forall \quad k = 1, 2, \ldots n_s \tag{43}$$

where $< \mathbf{u}, \mathbf{v} >= \mathbb{E}\{\mathbf{u}^T\mathbf{v}\}$ is the inner product. By using this condition and the expression for the residual, one has

$$\mathbb{E}\left\{\boldsymbol{\phi}_k^T(\theta)\left(\sum_{i=0}^{M_1}\mathbf{K}_i(\theta)\xi_i(\theta)\right)\left(\sum_{j=1}^{n_s}c_j\left(\frac{\boldsymbol{\phi}_j^T(\theta)\mathbf{f}_0}{\lambda_j(\theta)}\right)\boldsymbol{\phi}_j(\theta)\right)-\mathbf{f}_0\right\}=0 \qquad \forall \quad j=1,2,...n_s \quad \text{and} \quad k=1,2,...n_s \tag{44}$$

where $\mathbb{E}\{\blacksquare\}$ donates the expected value. For notational convenience, we can define $\alpha_j(\theta)=\frac{\boldsymbol{\phi}_j^T(\theta)\mathbf{f}_0}{\lambda_j(\theta)}$, thus it can be shown that Equation (44) can take the following form

$$\mathbb{E}\left\{\sum_{j=1}^{n_s}\sum_{i=0}^{M_1}\boldsymbol{\phi}_k^T(\theta)\mathbf{K}_i(\theta)\boldsymbol{\phi}_j(\theta)\xi_i(\theta)\alpha_j(\theta)c_j\right\}=\mathbb{E}\left\{\boldsymbol{\phi}_k^T(\theta)\mathbf{f}_0\right\} \tag{45}$$

By defining the vector $\mathbf{c}_{SA}=[c_1,c_2,\dots c_{n_s}]^T$, Equation (45) can be re-written as

$$\mathbb{E}\left\{\mathbf{Z}_{SA}(\theta)\right\}\mathbf{c}_{SA}=\mathbb{E}\left\{\mathbf{y}_{SA}(\theta)\right\} \qquad j,k=1,2,\dots,n_s \tag{46}$$

where $\mathbf{Z}_{SW_{kj}}(\theta)=\sum_{i=0}^{M_1}\left[\boldsymbol{\phi}_k^T(\theta)\mathbf{K}_i(\theta)\boldsymbol{\phi}_j(\theta)\right]\left[\xi_i(\theta)\alpha_j(\theta)\right];\ \forall j,k=1,2,\dots n_s$ and $\mathbf{y}_{SA}(\theta)=\boldsymbol{\phi}_k^T(\theta)\mathbf{f}_0$. The number of equations that need to be solved in order to calculate the unknown vector $\mathbf{c}(\omega,\theta)$ corresponds to the value of n_s. The arising expected values can be computed by using Monte Carlo simulations. Therefore by solving the set of linear equations given by Equation (46) the unknown coefficients can be obtained.

5.2. Sample-based Galerkin approach: Static load

In a similar manner to the previous approach, the solution vector has been modified to take the following form

$$\mathbf{u}_{SS}(\theta)\approx\sum_{j=1}^{n_s}d_j(\theta)\left(\frac{\boldsymbol{\phi}_j^T(\theta)\mathbf{f}_0}{\lambda_j(\theta)}\right)\boldsymbol{\phi}_j(\theta) \tag{47}$$

where $\lambda_j\in\mathbb{R}^{n_s}$ and $\boldsymbol{\phi}_j\in\mathbb{R}^{N\times n_s}$ represent the random eigenvalues and eigenvectors and $\mathbf{f}_0\in\mathbb{R}^N$ represents the deterministic excitation vector. Contrary to the previous approach, $d_j(\theta)\in\mathbb{R}^{n_s}$ are unknown constants that need to be computed for each realisation. The residual vector for this approach is defined as

$$\mathbf{r}_{SS}(\theta)=\mathbf{K}(\theta)\mathbf{u}_{SS}(\theta)-\mathbf{f}_0 \tag{48}$$

By making the residual orthogonal to a basis function, $d_j(\theta)$ can be computed. By using the same analogy as seen in the previous approach, the residual has been made orthogonal to a subset of random eigenvectors

$$< \mathbf{r}_{SS}(\theta), \boldsymbol{\phi}_k(\theta) > \qquad \forall \quad k = 1, 2, \dots n_s \tag{49}$$

Thus resulting in the following expression

$$\left\{ \boldsymbol{\phi}_k^T(\theta) \left(\sum_{i=0}^{M_1} \mathbf{K}_i(\theta) \xi_i(\theta) \right) \left(\sum_{j=1}^{n_s} d_j \left(\frac{\boldsymbol{\phi}_j^T(\theta) \mathbf{f}_0}{\lambda_j(\theta)} \right) \boldsymbol{\phi}_j(\theta) \right) - \mathbf{f}_0 \right\} = 0 \qquad \forall \quad j = 1, 2, \dots n_s \quad \text{and} \quad k = 1, 2, \dots n_s \tag{50}$$

For notational convenience, we define $\alpha_j(\theta) = \frac{\boldsymbol{\phi}_j^T(\theta) \mathbf{f}_0}{\lambda_j(\theta)}$. Therefore, the above expression can be manipulated to give

$$\sum_{j=1}^{n_s} \sum_{i=0}^{M_1} \left[\boldsymbol{\phi}_k^T(\theta) \mathbf{K}_i(\theta) \boldsymbol{\phi}_j(\theta) \right] \left[\xi_i(\theta) \alpha_j(\theta) d_j(\theta) \right] = \boldsymbol{\phi}_k^T(\theta) \mathbf{f}_0 \tag{51}$$

where $d_j(\theta)$ would be computed for each realisation. By defining the vector $\mathbf{d}_{SS}(\theta) = [d_1(\theta), d_2(\theta), \dots d_{n_s}(\theta)]^T$, Equation (51) can be simplified to

$$\mathbf{Z}_{SS}(\theta) \mathbf{d}_{SS}(\theta) = \mathbf{y}_{SS}(\theta) \qquad j, k = 1, 2, \dots, n_s \tag{52}$$

where $\mathbf{Z}_{SS_{kj}}(\theta) = \sum_{i=0}^{M_1} \left[\boldsymbol{\phi}_k^T(\theta) \mathbf{K}_i(\theta) \boldsymbol{\phi}_j(\theta) \right] \left[\xi_i(\theta) \alpha_j(\theta) \right]; \forall j, k = 1, 2, \dots n_s$ and $\mathbf{y}_{SS}(\theta) = \boldsymbol{\phi}_k^T(\theta) \mathbf{f}_0$. The number of equations that need to be solved in order to calculate the unknown vector $\mathbf{d}(\theta)$ corresponds to the value of n_s. Therefore, similarly to the sample-aggregated based Galerkin approach, the lower the dimension of the reduced system, the fewer the number of equations that need to be solved.

5.3. Sample-aggregated based Galerkin approach: Dynamic load

A similar approach to that seen in Section 5.1 can be implemented for incorporating a sample-aggregated based Galerkin error minimisation approach. The response vector for the case of a dynamic load has been modified to take the following form

$$\begin{aligned} \mathbf{u}_{DA}(\omega, \theta) &\approx \sum_{j=1}^{n_d} g_j(\omega) \left(\frac{\boldsymbol{\psi}_j^T(\theta) \tilde{\mathbf{f}}_0}{\omega_j^2(\theta) - \omega^2 + 2\mathrm{i}\omega_j(\theta)\omega\zeta} \right) \boldsymbol{\psi}_j(\theta) \\ &= \sum_{j=1}^{n_d} g_j(\omega) \beta_j(\omega, \theta) \boldsymbol{\psi}_j(\theta) \end{aligned} \tag{53}$$

Here $\beta_j(\omega,\theta)$ corresponds to the scalars introduced in Equation (25) and $g_j(\omega) \in \mathbb{C}^{n_d}$ are unknown constants that need to obtained for each $\omega \in \Omega$. In order to compute these unknown scalars, the residual obtained by computing the response by using Equation (53) can be projected onto the random undamped eigenvectors

$$< \mathbf{r}_{DA}(\omega,\theta), \boldsymbol{\psi}_k(\theta) > \qquad \forall \quad k = 1, 2, \ldots n_d \tag{54}$$

where

$$\mathbf{r}_{DA}(\omega,\theta) = \left(\sum_{i=0}^{M_2} \mathbf{D}_i(\omega)\xi_i(\theta) \right) \left(\sum_{j=1}^{n_d} g_j(\omega)\beta_j(\omega,\theta)\boldsymbol{\psi}_j(\theta) \right) - \tilde{\mathbf{f}}_0(\omega) \in \mathbb{C}^N \tag{55}$$

By following a similar approach to that seen in Section 5.1, the unknown constants g_j can be computed by solving the following set of linear equations

$$\mathbb{E}\left\{\mathbf{Z}_{DA}(\omega,\theta)\right\} \mathbf{g}_{DA}(\omega) = \mathbb{E}\left\{\mathbf{y}_{DA}(\omega,\theta)\right\} \qquad j,k = 1, 2, \ldots, n_d \tag{56}$$

where $\mathbf{Z}_{DA_{kj}}(\omega,\theta) = \sum_{i=0}^{M_2} \left[\boldsymbol{\psi}_k^T(\theta)\mathbf{D}_i(\omega)\boldsymbol{\psi}_j(\theta)\right] \left[\xi_i(\theta)\beta_j(\omega,\theta)\right];$

$$\beta_j(\omega,\theta) = \sum_{j=1}^{n_d} \left(\frac{\boldsymbol{\psi}_j^T(\theta)\tilde{\mathbf{f}}_0}{\omega_j^2(\theta) - \omega^2 + 2\mathrm{i}\omega_j(\theta)\omega\zeta} \right)$$

$$\mathbf{y}_{DA}(\omega,\theta) = \boldsymbol{\psi}_k^T(\theta)\tilde{\mathbf{f}}_0(\omega) \quad \forall \quad j,k = 1, 2, \ldots n_d$$

and $\mathbf{g}_{DA}(\omega)$ is a vector that contains the unknown constants $g_j(\omega)$

The expected values can be computed by utilising Monte Carlo simulations. The size of the linear system that needs to be solved corresponds to $n_d \times n_d$.

5.4. Sample-based Galerkin approach: Dynamic load

Similarly to the case of a static load, the response vector has been modified to take the following representation

$$\begin{aligned} \mathbf{u}_{DS}(\omega,\theta) &\approx \sum_{j=1}^{n_d} h_j(\omega,\theta) \left(\frac{\boldsymbol{\psi}_j^T(\theta)\tilde{\mathbf{f}}_0}{\omega_j^2(\theta) - \omega^2 + 2\mathrm{i}\omega_j(\theta)\omega\zeta} \right) \boldsymbol{\psi}_j(\theta) \\ &= \sum_{j=1}^{n_d} h_j\left(\omega,\theta\right) \beta_j\left(\omega,\theta\right) \boldsymbol{\psi}_j(\theta) \end{aligned} \tag{57}$$

The scalars $\beta_j(\omega,\theta)$ correspond to those seen in Equation (25) and $h_j\left(\omega,\theta\right) \in \mathbb{C}^{n_d}$ are unknown constants that need to be obtained for every realisation of each frequency. By

applying a sample-based Galerkin approach the unknown constants can be computed. By making the residual orthogonal to the random undamped eigenvectors, the unknown scalars $h_j(\omega,\theta)$ can be computed. By applying the same analogy as that seen in Section 5.2, it can be shown that the following set of equations need to be solved for every realisation of each frequency

$$\mathbf{Z}_{DS}(\omega,\theta)\mathbf{h}_{DS}(\omega) = \mathbf{y}_{DS}(\omega,\theta) \qquad j,k = 1,2,\ldots,n_d \tag{58}$$

where $$\mathbf{Z}_{DS_{kj}}(\omega,\theta) = \sum_{i=0}^{M_2} \left[\boldsymbol{\psi}_k^T(\theta)\mathbf{D}_i(\omega)\boldsymbol{\psi}_j(\theta)\right]\left[\xi_i(\theta)\beta_j(\omega,\theta)\right];$$

$$\beta_j(\omega,\theta) = \sum_{j=1}^{n_d}\left(\frac{\boldsymbol{\psi}_j^T(\theta)\tilde{\mathbf{f}}_0}{\omega_j^2(\theta)-\omega^2+2\mathrm{i}\omega_j(\theta)\omega\zeta}\right)$$

$$\mathbf{y}_{DS}(\omega,\theta) = \boldsymbol{\psi}_k^T(\theta)\tilde{\mathbf{f}}_0(\omega) \quad \forall \quad j,k = 1,2,\ldots n_d$$

and $\mathbf{h}_{DS}(\omega,\theta)$ is a vector that contains the unknown constants $h_j(\omega,\theta)$

The number of equations that need to be solved in order to calculate the unknown vector $\mathbf{h}_{DS}(\omega,\theta)$ corresponds to the value of n_d. It is imperative that the value of n_d is kept as low possible as a $n_d \times n_d$ sized set of linear equations needs to be solved for every realisation in each frequency step.

Let N correspond to the dimension of a stochastic finite element linear system and n_{samp} the number of Monte Carlo simulations under consideration. The total computational complexity incurred by directly solving Equation (3) is $n_{samp}\mathcal{O}(N^3)$. The same is true when solving Equation (4) for each frequency step. For both sample-based Galerkin approaches, the main contributions towards the computational complexities occur when inverting all of the $\mathbf{Z}_{SS}$ and $\mathbf{Z}_{DS}$ matrices. For the case of a static load, it can be deduced that the main contribution towards the computational complexity is $n_{samp}\mathcal{O}(N_s^3)$ where $N_s < N$. Likewise for the case of a dynamic load, for each frequency step it can be deduced that the main contribution towards the computational complexity is $n_{samp}\mathcal{O}(N_d^3)$ where $N_d < N$. However for the sample-aggregated based Galerkin approaches, the contributions due to inverting the $\mathbb{E}\{\mathbf{Z}_{SA}\}$ and $\mathbb{E}\{\mathbf{Z}_{DA}\}$ matrices are considerably less. For the case of a static load the contribution is $\mathcal{O}(N_s^3)$ where $N_s < N$, whilst for the case of a dynamic load the contribution is $\mathcal{O}(N_d^3)$ where $N_d < N$ for each frequency step.

The reduction in the computational complexity is due to the reduction in the number of inversions that need to be performed.

6. Application examples

Thus far four different methods for computing and approximating the responses of Equations (1) and (4) have been discussed:

- Directly solving in order to compute the benchmark solution (Equation (3) and (12)) [DMCS]
- Approximating the solution by projecting random scalars onto a stochastic basis (Equations (37) and (40)) [SP]
- Approximating the solution by projecting a random scalar onto a stochastic basis (including a sample-aggregated based Galerkin error minimisation approach) (Equations (41) and (53)) [SPAG]
- Approximating the solution by projecting a random scalar onto a stochastic basis (including a sample-based Galerkin error minimisation approach) (Equations (47) and (57)) [SPSG]

This section aims to apply and compare the proposed methods by utilising a physical structure. Subsequently the four methods are applied to analyse the bending of a Euler-Bernoulli cantilever beam that has stochastic parameters. The analysis has been conducted separately for when the cantilever beam is subjected to a static load and for when the cantilever beam is subjected to a dynamic load. The effectiveness of the approximation methods are subsequently scrutinised for both cases. The length of the cantilever beam under consideration is 0.80 m, and its cross-section is a rectangle of width 0.035 m and height 0.0035 m. Figure 1 illustrates the system.

By using a stochastic finite element method the cantilever beam has been discretized into 80 elements. For the deterministic case, the Young's modulus is $E = 2 \times 10^{11}$ Nm^{-2} thus corresponding to a steel beam. The deterministic second moment of area of the beam

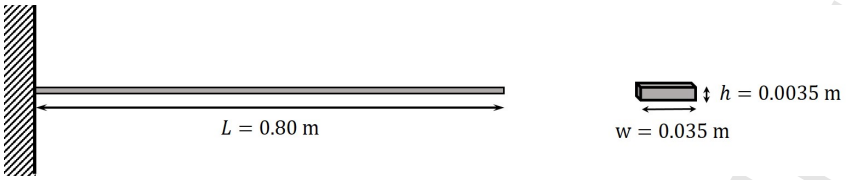

Fig. 1: The configuration of the cantilever beam

is $I = 1.25 \times 10^{-10}$ m^4. The bending rigidity of the beam, EI, has been assumed to be a random field of the following form

$$EI(x, \theta) = \overline{EI}(1 + a(x, \theta)) \tag{59}$$

where x corresponds to the position along the length of the cantilever beam and $\overline{EI}$ corresponds to the mean of the bending rigidity. The random field $a(x, \theta)$ is assumed to be an uniform random field with correlation length $\mu_a = L/2$ where L is the length of the cantilever beam. Each of the projection methods have been simulated 10,000 times and the performances of the approximation methods have been compared with that of the DMCS approach. $10,000$ samples gives a satisfactory convergence of the first two moments of the quantities of interest for both the static load and dynamic load cases. Both cases have been modelled for two different values of the standard deviation of the bending rigidity: $\sigma_a = \{0.05, 0.25\}$. This allows the methods to be compared under different levels of uncertainty.

6.1. Cantilever beam: Static load

For the case of a static load a 1.00 N deterministic vertical point load is applied at the free end of the cantilever beam. All three stochastic projection methods have been truncated to include the first 4 terms, hence $n_s = 4$. This implies that 156 terms have been discarded from each of the summations. In addition to the matrix that contributes to the deterministic nature of the random stiffness matrix, four general matrix are used in conjunction with the random variables ξ_i to model the random stiffness matrices. It has been proven that the displacement of the beam can be normalised by $\frac{f_0 L^3}{3EI}$ to ensure that the deterministic vertical displacement has a value of 1 at the tip of the cantilever beam.

Figures 2a and 2b illustrate the mean of the normalised vertical displacement at all nodes of the beam for both values of σ_a. When $\sigma_a = 0.05$ no visible difference can be seen

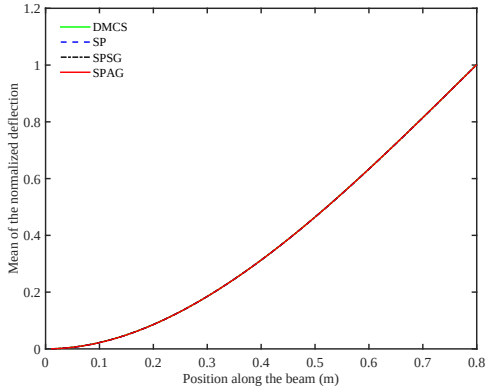

(a) The mean of the normalised vertical displacement: $\sigma_a = 0.05$

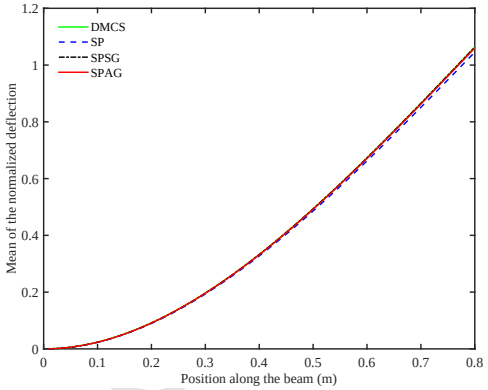

(b) The mean of the normalised vertical displacement: $\sigma_a = 0.25$

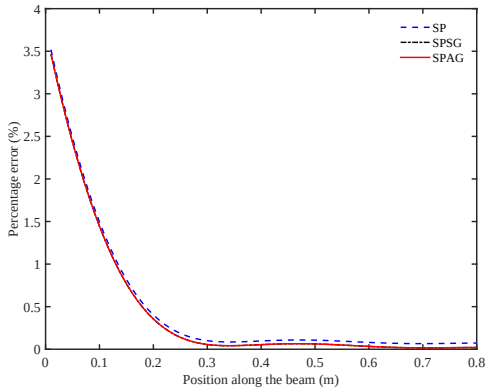

(c) The percentage error of the mean of the normalised vertical displacement: $\sigma_a = 0.05$

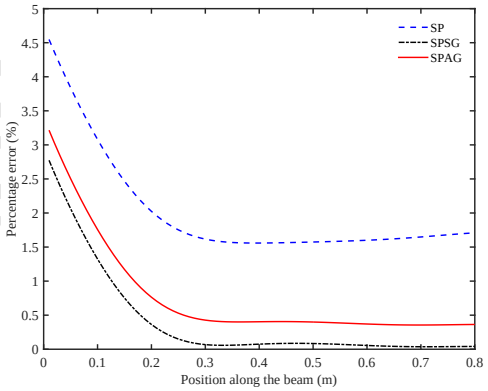

(d) The percentage error of the mean of the normalised vertical displacement: $\sigma_a = 0.25$

Fig. 2: The mean of the normalised vertical displacement of the cantilever beam and a comparison of the percentage error of the mean of the normalised vertical displacement for $\sigma_a = \{0.05, 0.25\}$.

between the different methods, however when $\sigma_a = 0.25$ a slight discrepancy can be seen between the SP and the other methods. In order to further analyse the discrepancy, the percentage error of the mean of the vertical displacement is explored. This is represented by

$$\varepsilon_{\%} = 100 \times \frac{|MDMCS - MCOMP|}{MDMCS} \tag{60}$$

where MDMCS indicates the mean of the DMCS approach, and MCOMP the mean of the comparable methods. The discrepancy between the SP method and the Galerkin methods is apparent in Figure 2d. It is apparent that both Galerkin methods lower the error in the mean of the vertical displacement, however the SPSG method slightly outperforms the SPAG method.

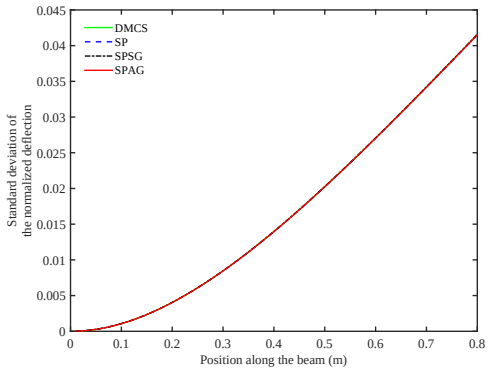

(a) The standard deviation of the normalised vertical displacement: $\sigma_a = 0.05$

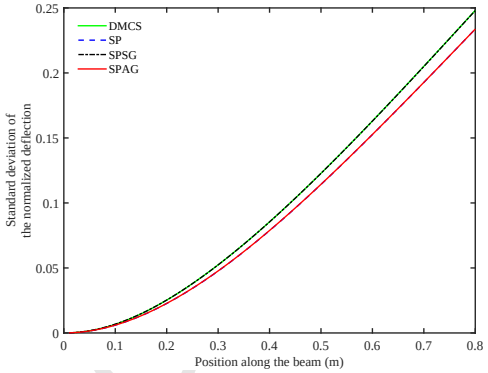

(b) The standard deviation of the normalised vertical displacement: $\sigma_a = 0.25$

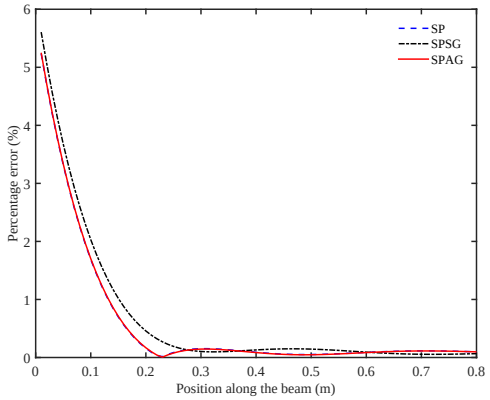

(c) The percentage error of the standard deviation of the normalised vertical displacement: $\sigma_a = 0.05$

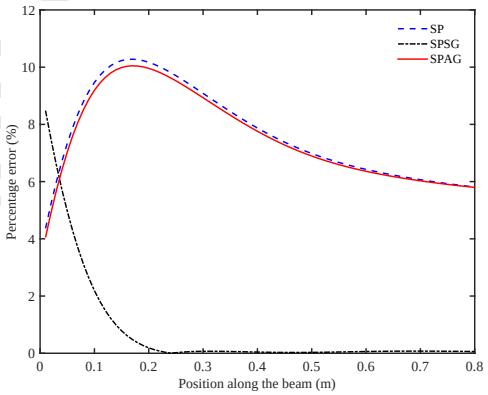

(d) The percentage error of the standard deviation of the normalised vertical displacement: $\sigma_a = 0.25$

Fig. 3: The standard deviation of the normalised vertical displacement of the cantilever beam and a comparison of the percentage error of the standard deviation of the normalised vertical displacement for $\sigma_a = \{0.05, 0.25\}$.

The normalised standard deviation of the vertical displacement of the cantilever beam is illustrated for all nodes in Figures 3a and 3b. All methods seem to capture the standard deviation of the benchmark method well when $\sigma_a = 0.05$, however this is not the case when $\sigma_a = 0.25$. The percentage error of the standard deviation of the vertical displacement is explored to further compare the methods. The percentage error has been defined as follows

$$\epsilon_{\%} = 100 \times \frac{|SDMCS - SCOMP|}{SDMCS} \tag{61}$$

where SDMCS indicates the standard deviation of the DMCS approach, and SCOMP the standard deviation of the comparable methods. Contrary to the mean, for the case of

$\sigma_a = 0.25$ a vast difference is apparent between the standard deviation of the SPSG and SPAG methods. Barring the initial 0.06 m of the cantilever beam, the SPSG dramatically reduces the percentage error of the standard deviation. Although applying the SPAG lowers the percentage error along the cantilever beam, the reduction is small.

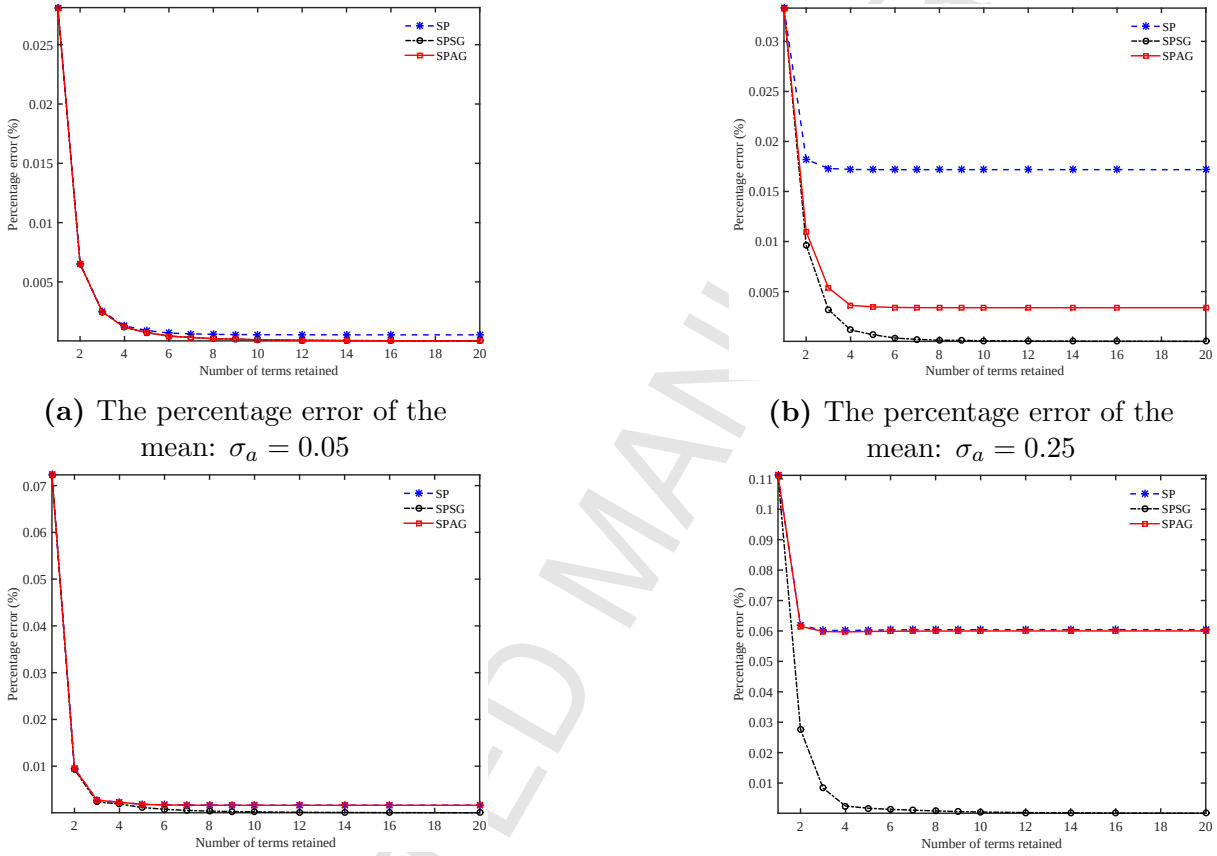

(a) The percentage error of the mean: $\sigma_a = 0.05$

(b) The percentage error of the mean: $\sigma_a = 0.25$

(c) The percentage error of the standard deviation: $\sigma_a = 0.05$

(d) The percentage error of the standard deviation: $\sigma_a = 0.25$

Fig. 4: A comparison of the percentage errors of the mean and standard deviation of the vertical tip displacement for different values of n_s when $\sigma_a = \{0.05, 0.25\}$.

In Figure 4 the percentage error of the mean and the standard deviation of the vertical displacement at the tip of the cantilever beam is further assessed for different values of n_s i.e. the number of terms retained in Equations (37), (47) and (41). As expected, for each method the percentage error decreases as additional terms are retained in the summations. It is apparent that both the Galerkin methods significantly lowers the percentage error of the mean in comparison to the SP method. However the performances of the Galerkin methods differ considerably when assessing the percentage error of the standard deviation.

The SPSG method considerably lowers the percentage error of the standard deviation. Only a very small reduction is seen when the SPAG method is used in comparison to the SP method.

6.2. Cantilever beam: Dynamic load

For the case of a dynamic load, an unit amplitude harmonic point load is applied at the free tip of the beam. This is applied over a frequency range of $0-500$ Hz at an interval of 2 Hz. The constant modal damping model has a 1.5% damping factor for each of the modes. Initially n_d has been set to 10 thus implying that 10 terms have been retained in Equations (25), (53) and (57). Similarly to the static case four general matrices (K_i where $i = 1, 2, 3, 4$) are used in conjunction with the random variables ξ_i and deterministic matrix K_0 to model the random stiffness matrices. The mass matrix is assumed to be deterministic.

The mean vertical amplitude at the tip of the cantilever beam is illustrated over the stated frequency range in Figures 5a and 5b for both $\sigma_a = 0.05$ and $\sigma_a = 0.25$. The deterministic vertical amplitude is also illustrated [DET]. In order to analyse the error arising from the mean of the response vector, the approximate L^2 relative error is considered. This ensures that the error arising for a given frequency can be characterised by a single value. The approximate L^2 relative error of the mean of the response vector for each frequency step has been defined as follows

$$\hat{\varepsilon}^{\boldsymbol{\mu}}_{L^2}(\omega) = \frac{||\boldsymbol{\mu}_{DMCS}(\omega) - \boldsymbol{\mu}_{CM}(\omega)||_{L^2}}{||\boldsymbol{\mu}_{DMCS}(\omega)||_{L^2}} \tag{62}$$

where $\boldsymbol{\mu}_{DMCS}$ denotes the mean of the response vector obtained by using the DMCS method and $\boldsymbol{\mu}_{CM}$ the mean of the response vector obtained by a comparable method. Although decreases are apparent, the SPAG method does not always decrease the error. Increases are visibly apparent in comparison to the SP method at large valued resonance frequencies. On the other hand the SPSG method always decreases the L^2 relative error of the mean. This is most apparent at the systems' resonance values.

Figures 6a and 6b depict the standard deviation of the vertical amplitude at the tip of the beam for both values of σ_a. In a similar manner to the case of the mean, the approximate L^2 relative error of the standard deviation of the response vector is defined

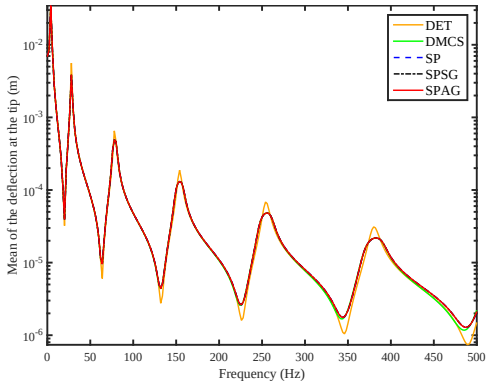

(a) The mean of the vertical amplitude at the tip of the cantilever beam: $\sigma_a = 0.05$

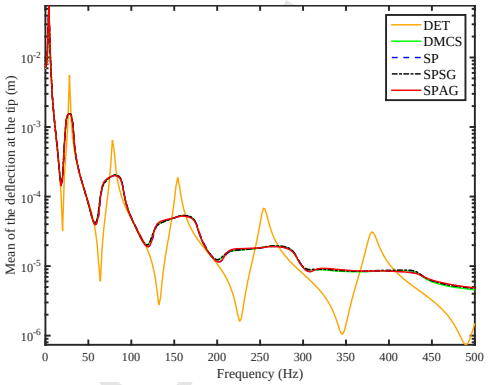

(b) The mean of the vertical amplitude at the tip of the cantilever beam: $\sigma_a = 0.25$

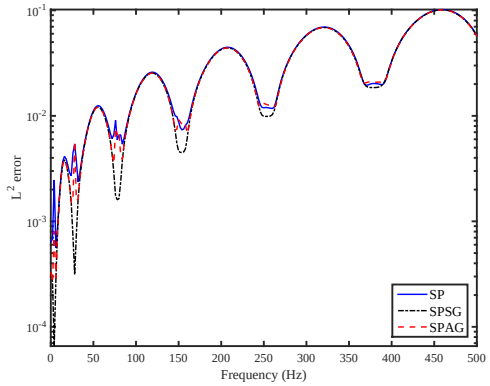

(c) The L^2 relative error of the mean of the response vector: $\sigma_a = 0.05$

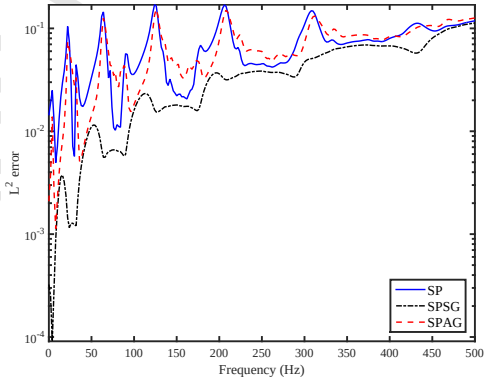

(d) The L^2 relative error of the mean of the response vector: $\sigma_a = 0.25$

Fig. 5: The mean of the vertical amplitude is observed at the tip of the cantilever beam in conjunction with the L^2 relative error of the mean of the response vector at each frequency step. These are illustrated for $\sigma_a = \{0.05, 0.25\}$.

as follows

$$\hat{\varepsilon}_{L^2}^{\boldsymbol{\sigma}}(\omega) = \frac{||\boldsymbol{\sigma}_{DMCS}(\omega) - \boldsymbol{\sigma}_{CM}(\omega)||_{L^2}}{||\boldsymbol{\sigma}_{DMCS}(\omega)||_{L^2}} \tag{63}$$

where $\boldsymbol{\sigma}_{DMCS}$ denotes the standard deviation of the response vector obtained by using the DMCS method and $\boldsymbol{\sigma}_{CM}$ denotes the standard deviation of the response vector obtained by a comparable method. When $\sigma_a = 0.05$ it's apparent that the SPAG method slightly lowers the L^2 relative error of the standard deviation for the majority of frequencies. However when $\sigma_a = 0.25$ the effectiveness of the SPAG method is suspect due to the L^2 relative error rising at numerous frequencies in comparison to the SP method. Nevertheless the SPSG method lowers the L^2 relative error at all frequencies for both values of σ_a.

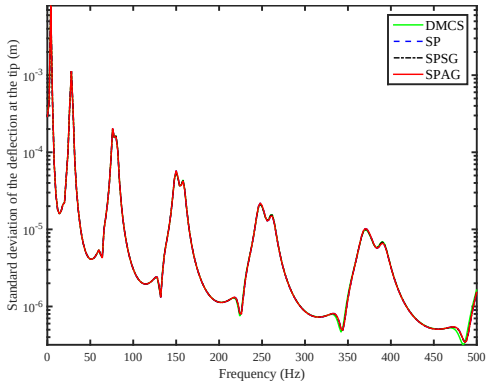

(a) The standard deviation of the vertical amplitude at the tip of the cantilever beam: $\sigma_a = 0.05$

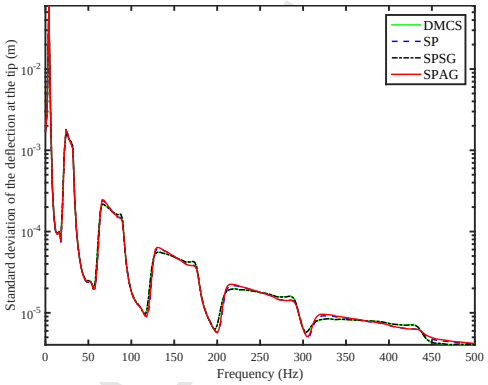

(b) The standard deviation of the vertical amplitude at the tip of the cantilever beam: $\sigma_a = 0.25$

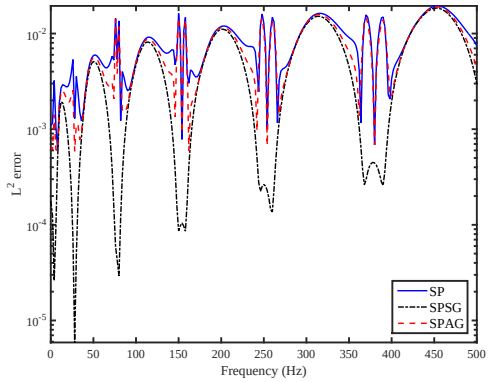

(c) The L^2 relative error of the standard deviation of the response vector: $\sigma_a = 0.05$

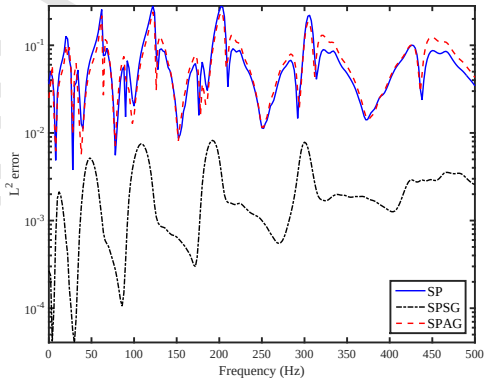

(d) The L^2 relative error of the standard deviation of the response vector: $\sigma_a = 0.05$

Fig. 6: The standard deviation of the vertical amplitude is observed at the tip of the cantilever beam in conjunction with the L^2 relative error of the standard deviation of the response vector at each frequency step. These are illustrated for $\sigma_a = \{0.05, 0.25\}$.

The probability density function of the vertical amplitude of the displacement at the tip of the beam is illustrated by Figure 7 for both vales of σ_a at a frequency of 154 Hz. This frequency value corresponds to the fourth resonance frequency of the cantilever beam.

Figure 8 depicts the log of the approximate L^2 relative error of the mean of the response vector for different values of n_d. This is depicted for each of the frequency steps and for both values of σ_a. The troths arising in the contour plots of the relative errors correspond to the resonance values, thus it can be deduced that the error is larger at adjacent anti-resonance values. As expected, the trend of the approximate relative error increases with frequency. This is due to the higher order terms becoming more important at the higher frequencies. Both Galerkin approaches seem to lower the relative error of the mean in

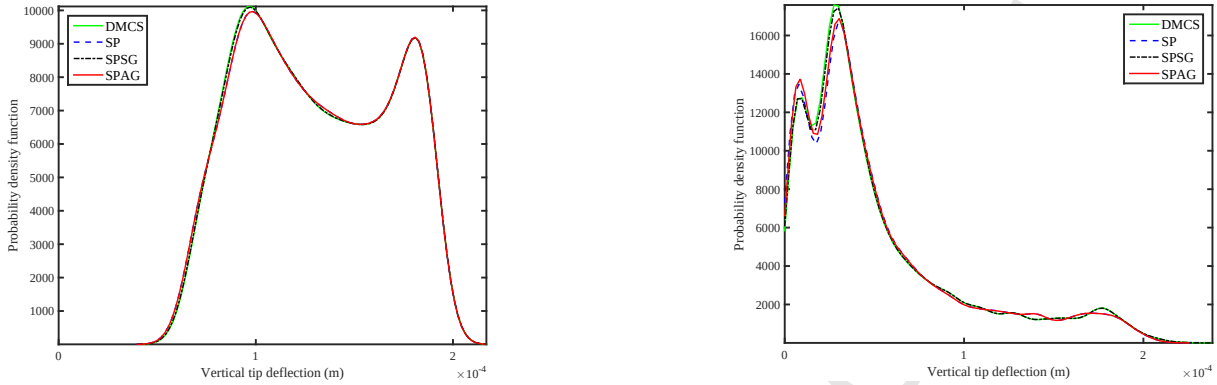

(a) Pdf: $\sigma_a = 0.05$ **(b)** Pdf: $\sigma_a = 0.25$

Fig. 7: The probability density functions of the vertical amplitude when an unit harmonic point load of 154 Hz is asserted at the tip of the cantilever beam. The probability density functions are illustrated for $\sigma_a = \{0.05, 0.25\}$.

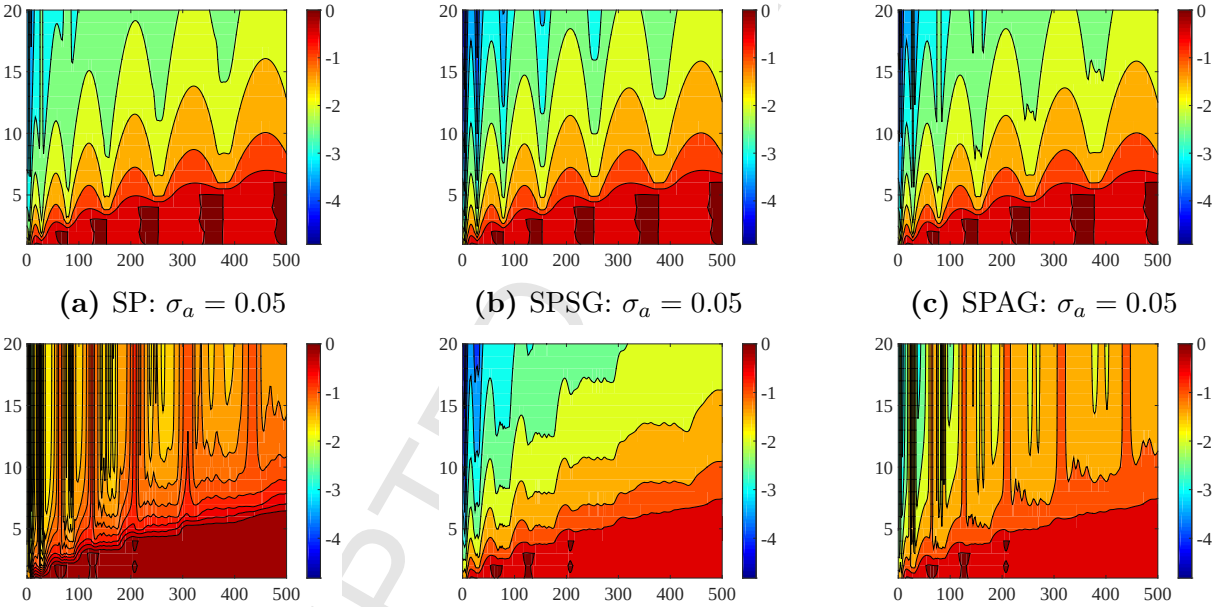

(a) SP: $\sigma_a = 0.05$ **(b)** SPSG: $\sigma_a = 0.05$ **(c)** SPAG: $\sigma_a = 0.05$

(d) SP: $\sigma_a = 0.25$ **(e)** SPSG: $\sigma_a = 0.25$ **(f)** SPAG: $\sigma_a = 0.25$

Fig. 8: The log of the L^2 relative error of the mean of the response vector. The contour plots depict the log of the L^2 relative error for different values of n_d at each frequency step for $\sigma_a = \{0.05, 0.25\}$.

general, however the SPSG method significantly outperforms the SPAG method when $\sigma_a = 0.25$.

The log of the approximate L^2 relative error of the standard deviation of the response vector is illustrated for different values of n_d at each frequency step in Figure 9. A slight reduction is seen in the relative error at low frequencies when the SPAG method

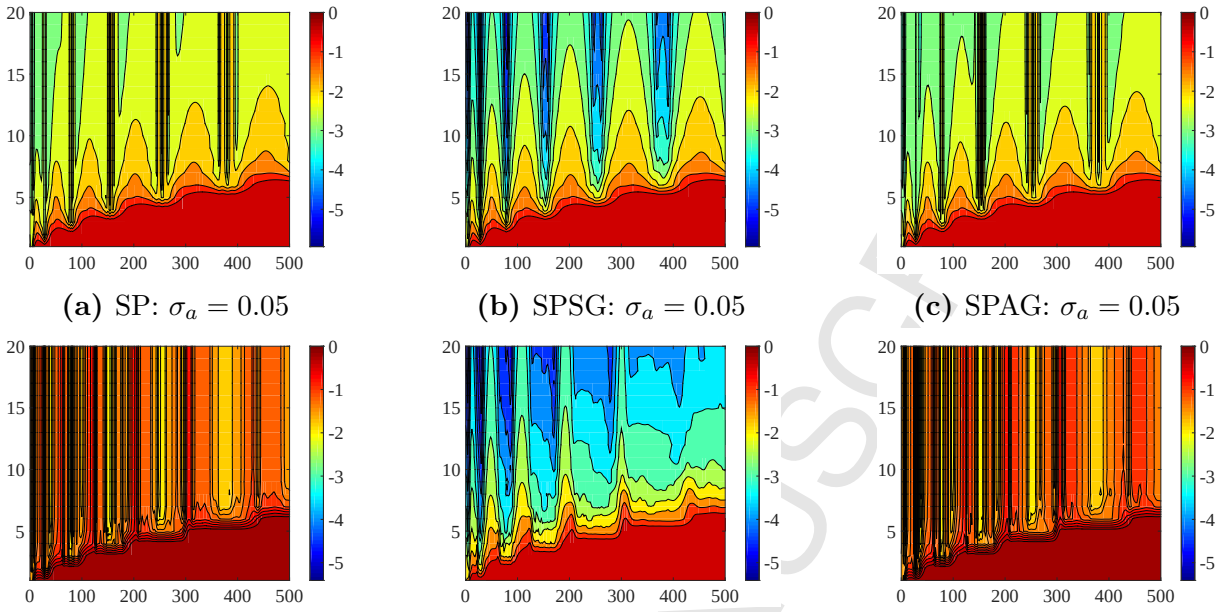

(a) SP: $\sigma_a = 0.05$ **(b)** SPSG: $\sigma_a = 0.05$ **(c)** SPAG: $\sigma_a = 0.05$

(d) SP: $\sigma_a = 0.25$ **(e)** SPSG: $\sigma_a = 0.25$ **(f)** SPAG: $\sigma_a = 0.25$

Fig. 9: The log of the L^2 relative error of the standard deviation of the response vector. The contour plots depict the log of the L^2 relative error for different values of n_d at each frequency step for $\sigma_a = \{0.05, 0.25\}$.

is applied, however at larger frequencies the SPAG method increases the relative error of the standard deviation in comparison to the SP method. This is evidently visible when $\sigma_a = 0.25$. A large reduction in the relative error of the standard deviation is seen when the SPSG method is applied. This can be observed at both values of σ_a.

7. Summary and Conclusions

7.1. Summary

Two approaches which incorporate different Galerkin projection schemes have been suggested to calculate the response of discretized stochastic partial differential equations. By utilising the random eigenvalue problem, it has been proven that the response vector of discretized structures subjected to static or dynamic loads can be represented by a summation. Due to the high computational cost associated with calculating the exact solutions, reduced approaches have been proposed where random eigenvalues and eigenvectors are approximated and low valued terms discarded. Consequently two multiplicative Galerkin error minimisation approaches have been presented. The first being a sample-based Galerkin projection scheme and the other being a sample-aggregated based

Galerkin projection scheme. The two novel novel Galerkin projection schemes presented in the paper are subsequently used to analyse the response of a stochastic Euler-Bernoulli cantilever beam undergoing both a static and a dynamic load.

7.2. Conclusions

Following the application of the methods to analyse a stochastic Euler-Bernoulli cantilever beam, the following conclusions have been established:

The cantilever beam subjected to a static load

- Both Galerkin schemes lower the error arising in the mean of the response.
- It is only the sample-based Galerkin projection scheme that substantially lowers the error arising in the standard deviation of the response.

The cantilever beam subjected to a dynamic load

- At low frequencies both Galerkin schemes lower the error arising in the mean of the response. Both methods also lower the error induced in standard deviation, however the sample-based Galerkin projection scheme substantially outperforms the sample-aggregated based Galerkin projection scheme.
- At high frequencies the sample-aggregated based Galerkin projection scheme introduces additional error in both the mean and standard deviation of the response.
- The sample-based Galerkin projection scheme lowers the error in both the mean and standard deviation of the response at low and high valued frequencies.
- When the sample-based Galerkin projection scheme is utilised, a substantial reduction in the L^2 relative error is seen in both the mean and standard deviation of the response at the resonance values in comparison with neighbouring anti-resonance values.

Further work in this field would include developing methods to compute optimal bases in order to produce new efficient reduced-order methods.

8. Acknowledgements

The authors acknowledge the financial support received from Engineering Research Network Wales (one of three Sêr Cymru National Research Networks).

References

[1] M. Papadrakakis, V. Papadopoulos, Robust and efficient methods for stochastic finite element analysis using Monte Carlo simulation, Computer Methods in Applied Mechanics and Engineering 134 (3-4) (1996) 325–340.

[2] H. J. Pradlwarter, G. I. Schuëller, On advanced Monte Carlo simulation procedures in stochastic structural dynamics, International Journal of Non-Linear Mechanics 32 (4) (1997) 735 – 744, Third International Stochastic Structural Dynamics Conference.

[3] A. Kreinin, L. Merkoulovitch, D. Rosen, M. Zerbs, Principal component analysis in Quasi Monte Carlo simulation, Algo Research Quarterly 2 (2) (1998) 21–29.

[4] I. G. Graham, F. Y. Kuo, J. A. Nichols, R. Scheichl, C. Schwab, I. H. Sloan, Quasi-monte carlo finite element methods for elliptic pdes with lognormal random coefficients, Numerische Mathematik 131 (2) (2015) 329–368.

[5] J. C. Helton, F. J. Davis, Latin hypercube sampling and the propagation of uncertainty in analyses of complex systems, Reliability Engineering & System Safety 81 (1) (2003) 23–69.

[6] K. dos Santos, A. Beck, K. dos Santos, A. Beck, A benchmark study on intelligent sampling techniques in Monte Carlo simulation, Latin American Journal of Solids and Structures 12 (4) (2015) 624–648.

[7] D. Lucor, C.-H. Su, G. E. Karniadakis, Generalized polynomial chaos and random oscillators, International Journal for Numerical Methods in Engineering 60 (3) (2004) 571–596.

[8] Z. Yimin, S. Chen, Q. Liu, T. Liu, Stochastic perturbation finite elements, Computers and Structures 59 (3) (1996) 425 – 429.

[9] B. S. Lazarov, M. Schevenels, O. Sigmund, Topology optimization with geometric uncertainties by perturbation techniques, International Journal for Numerical Methods in Engineering 90 (11) (2012) 1321–1336.

[10] F. Yamazaki, M. Shinozuka, G. Dasgupta, Neumann expansion for stochastic finite element analysis, Journal of Engineering Mechanics-ASCE 114 (8) (1988) 1335–1354.

[11] C. R. Á. da Silva, A. T. Beck, A Fast Convergence Parameter for Monte CarloNeumann Solution of Linear Stochastic Systems, ASCE-ASME J. Risk and Uncert. in Engrg. Sys., Part B: Mech. Engrg. 1 (2) (2015) 021002.

[12] N. Wiener, The homogeneous chaos, American Journal of Mathematics 60 (4) (1938) 897–936.

[13] R. G. Ghanem, P. D. Spanos, Stochastic Finite Elements: A Spectral Approach (revised edition), Dover Publications Inc., 2012.

[14] J. Yang, B. Faverjon, H. Peters, N. Kessissoglou, Application of Polynomial Chaos Expansion and Model Order Reduction for Dynamic Analysis of Structures with Uncertainties, Procedia IUTAM 13 (2015) 63–70.

[15] K. Sepahvand, S. Marburg, Stochastic Dynamic Analysis of Structures with Spatially Uncertain Material Parameters, International Journal of Structural Stability and Dynamics 14 (08) (2014) 1440029.

[16] D. B. Xiu, G. E. Karniadakis, The wiener-askey polynomial chaos for stochastic differential equations, Siam Journal on Scientific Computing 24 (2) (2002) 619–644.

[17] D. B. Xiu, G. E. Karniadakis, Modeling uncertainty in flow simulations via generalized polynomial chaos, Journal of Computational Physics 187 (1) (2003) 137–167.

[18] S. K. Sachdeva, P. B. Nair, A. J. Keane, Comparative study of projection schemes for stochastic finite element analysis, Computer Methods in Applied Mechanics and Engineering 195 (19-22) (2006) 2371–2392.

[19] P. B. Nair, A. J. Keane, Stochastic Reduced Basis Methods, AIAA Journal 40 (8) (2002) 1653–1664.

[20] S. Adhikari, C. S. Manohar, Dynamic analysis of framed structures with statistical uncertainties, Int. J. Numer. Meth. Engng 44 (1999) 1157–1178.
[21] S. Huang, S. Mahadevan, R. Rebba, Collocation-based stochastic finite element analysis for random field problems, Probabilistic Engineering Mechanics 22 (2) (2007) 194–205.
[22] B. Ganis, H. Klie, M. F. Wheeler, T. Wildey, I. Yotov, D. Zhang, Stochastic collocation and mixed finite elements for flow in porous media, Computer Methods in Applied Mechanics and Engineering 197 (43-44) (2008) 3547–3559.
[23] A. Kundu, F. DiazDelaO, S. Adhikari, M. Friswell, A hybrid spectral and metamodeling approach for the stochastic finite element analysis of structural dynamic systems, Computer Methods in Applied Mechanics and Engineering 270 (2014) 201–219.
[24] R. Chowdhury, S. Adhikari, High dimensional model representation for stochastic finite element analysis, Applied Mathematical Modelling 34 (12) (2010) 3917–3932.
[25] A. Kundu, S. Adhikari, Dynamic analysis of stochastic structural systems using frequency adaptive spectral functions, Probabilistic Engineering Mechanics 39 (2015) 23–38.
[26] A. Kundu, S. Adhikari, Transient Response of Structural Dynamic Systems with Parametric Uncertainty, Journal of Engineering Mechanics 140 (2) (2014) 315–331.
[27] A. Nouy, Recent developments in spectral stochastic methods for the numerical solution of stochastic partial differential equations, Archives of Computational Methods in Engineering 16 (2009) 251–285.
[28] S. Daouk, F. Louf, O. Dorival, L. Champaney, S. Audebert, Uncertainties in structural dynamics: overview and comparative analysis of methods, Mechanics & Industry 16 (4) (2015) 404.
[29] E. Jacquelin, S. Adhikari, J.-J. Sinou, M. I. Friswell, Polynomial Chaos Expansion and Steady-State Response of a Class of Random Dynamical Systems, Journal of Engineering Mechanics 141 (4) (2015) 04014145.
[30] S. Adhikari, Structural Dynamic Analysis with Generalized Damping Models: Analysis, Wiley ISTE, UK, 2013.
[31] G. S. Szekely, G. I. Schueller, Computational procedure for a fast calculation of eigenvectors and eigenvalues of structures with random properties, Computer Methods in Applied Mechanics and Engineering 191 (8-10) (2001) 799–816.
[32] R. Ghanem, D. Ghosh, Efficient characterization of the random eigenvalue problem in a polynomial chaos decomposition, International Journal for Numerical Methods in Engineering 72 (4) (2007) 486–504.
[33] S. Adhikari, Structural dynamic analysis with generalized damping models : identification, Mechanical Engineering and Solid Mechanics Series, Wiley - ISTE, London, 2014.